Publ. Astron. Soc. Japan (2019) 71 (1), 19 (1–10)
doi: 10.1093/pasj/psy139
Advance Access Publication Date: 2019 January 8

Property of young massive clusters in a galaxy–galaxy merger remnant

Hidenori Matsui,[1,2,*] Ataru Tanikawa,[2,3] and Takayuki R. Saitoh[4]

[1]National Institute of Technology, Asahikawa College, Shunkodai 2-2-1-6, Asahikawa, Hokkaido 071-8142, Japan
[2]Department of Earth Science and Astronomy, College of Arts and Sciences, The University of Tokyo, 3-8-1 Komaba, Meguro-ku, Tokyo 153-8902, Japan
[3]RIKEN Advanced Institute for Computational Science, 7-1-26 Minatojima-minami-machi, Chuo-ku, Kobe, Hyogo 650-0047, Japan
[4]Earth-Life Science Institute, Tokyo Institute of Technology, 2-12-1 Ookayama, Meguro, Tokyo 152-8551, Japan

*E-mail: matsui@asahikawa-nct.ac.jp

Received 2018 October 12; Accepted 2018 November 12

Abstract

We investigate the properties of young massive clusters (YMCs) in a galaxy–galaxy merger remnant by analyzing the data obtained by a gas-rich major merger simulation in Matsui et al. (2012, ApJ, 746, 26). We found that the YMCs are distributed at a few kpc and at ∼10 kpc from the galactic center; in other words, there are two components of their distribution. The former are formed in filamentary and turbulent gas generated at a few kpc from the center as a result of galaxy encounters, and the latter are formed in tidal tails which are far from the center. The YMCs are much less concentrated than galaxy stars. The mass function of the YMCs is $dN/dM \propto M^{-2}$. Most YMCs are formed between the second encounter and the final coalescence phase of the galactic cores, and their formation rate is especially high at the final coalescence phase. Most of them consist of single stellar population in age, but YMCs with multi-stellar populations in age are also formed. The multiple populations are produced by the following process: a YMC captures dense gas, and another generation of stars form within the cluster. There are several YMCs formed in an isolated disk before the encounter of galaxies. These candidates contain stars with various ages by capturing dense gas and forming stars. YMCs in a merger remnant have various orbits, but a large fraction of candidates have circular orbits.

Key words: galaxies: evolution — galaxies: formation — galaxies: interactions — galaxies: structure — methods: numerical

1 Introduction

Major mergers of gas-rich galaxies are expected to play an important role in the formation of globular clusters. The CO observation of local interacting galaxies showed a compressed gas filament, which may lead to formations of globular clusters, induced by galaxy–galaxy collision (Kaneko et al. 2018). The optical and infrared images found young massive star clusters with $\sim 10^{5-6}\,M_{\odot}$ formed in the galaxy–galaxy merging process (Whitmore & Schweizer

1995; Whitmore et al. 1999; Mengel et al. 2008). In galaxy–galaxy merger remnants, globular cluster systems formed in a galaxy–galaxy merging process are detected (Bassino & Caso 2017; Ko et al. 2018). In order to study formation, evolution, and properties of such globular cluster systems in more detail, numerical simulations of a galaxy–galaxy merger are needed.

Previously, a large number of numerical simulations of the galaxy mergers have been performed (Mihos & Hernquist 1996; Barnes & Hernquist 1996; Kazantzidis et al. 2005; Cox et al. 2006; Di Matteo et al. 2007). These numerical simulations succeeded to roughly understand dynamics in the galaxy–galaxy merging process such as gas inflow to the galactic central region or a central starburst. These studies, however, were not easily able to reproduce shock-induced star and star cluster formations in the merging process as shown by observations. This is because they used an unrealistic interstellar medium (ISM) model with temperature cutoff at $T = 10^4$ K in a cooling function due to the limited mass and spatial resolution. The artificial high temperature floor of ISM prevents ISM from gravitational instability at the shock generated by the galaxy–galaxy encounter.

In order to investigate formations of star clusters in the galaxy–galaxy merging process, a subgrid model for star clusters is used instead of resolving the formations of individual star clusters directly (Bekki et al. 2002; Kruijssen et al. 2012). Bournaud, Duc, and Emsellem (2008) have performed high-resolution simulations of merging galaxies and reproduced formations of star clusters directly, although they used a method of sticky particles instead of resolving hydrodynamics.

Recently, the higher mass and spatial resolution simulations of merging galaxies have been performed (Saitoh et al. 2009; Kim et al. 2009; Teyssier et al. 2010; Matsui et al. 2012; Hopkins et al. 2013a, 2013b; Renaud et al. 2015). The high-resolution simulations allow us to take radiative cooling of low-temperature gas ($T < 10^4$ K) into account and realize the multi-phase nature of ISM. These simulations have naturally succeeded to reproduce shock-induced star and star cluster formations. These studies have clarified shock-induced star cluster formations at the first encounter of galaxies (Saitoh et al. 2009, 2010), formations of hypermassive star clusters in the galaxy–galaxy merging process (Matsui et al. 2012), and the formation mechanism of star clusters at each interaction stage (Renaud et al. 2015). The formation of globular clusters in merging galaxies at high redshift are also clarified by cosmological simulations (Kim et al. 2018). Although formations of star clusters in the merging process were clarified, the properties of globular clusters in a merger remnant have not been analyzed yet.

In this paper, we focus on and investigate the properties of young massive cluster (YMCs) formed in the galaxy–galaxy merging process, which can produce luminous infrared galaxies (LIRGs) as shown in Matsui et al. (2012, hereafter Paper I). For this purpose, we analyze a galaxy–galaxy merger remnant obtained in Paper I. We describe our methods in section 2 and results in section 3. Summary and discussions are presented in section 4.

2 Method

2.1 Simulation data

To investigate a merger remnant and YMCs in that remnant, simulation data obtained by Paper I is analyzed. Here, the simulations have been performed by the Tree+GRAPE smoothed particles hydrodynamics (SPH)/N-body code "ASURA" (Saitoh et al. 2008). We analyze mainly the data of the highest resolution model, called $H_{\rm TT,\,5pc}$. In this model, the initial setup is as follows. First, we simulate an isolated disk galaxy, which consists of an exponential disk with $6.3 \times 10^9\,M_\odot$ and a dark matter halo with $1.1 \times 10^{11}\,M_\odot$, for 1000 Myr. The initial disk and halo include gas, the metallicity of which is 0.01, with $1.2 \times 10^9\,M_\odot$ and $1.1 \times 10^9\,M_\odot$, respectively. The initial metallicity is slightly less than solar metallicity and is larger than that of the Large Magellanic Cloud (Choudhury et al. 2016). After stabilizing the disk, we start galaxy–galaxy merger simulations in which both disks are tilted at -109° and 71° to the orbital plane, respectively, and prograde–prograde encounter occurs. We set the start time of the merger simulation to be $t = 0$. At $t = 0$, each galaxy includes gas with $1.5 \times 10^9\,M_\odot$ since the gas decreases due to star formation. Hereafter, initial stars at $t = -1000$ Myr are called "pre-existing stars", newly born stars before $t = 0$ are "old stars", and stars born after $t = 0$ are "new stars". After starting the merger simulation, the first, second, and third encounters occur at $t \sim 450$ Myr, $t \sim 850$ Myr, and $t \sim 1000$ Myr, respectively. See Paper I for details.

In the $H_{\rm TT,\,5pc}$ model, the numbers of SPH particles, pre-existing- and old-star particles, and dark matter particles at $t = 0$ are 442958, 2051314, and 27720000, respectively. The mass and gravitational softening length of SPH particles are $7.5 \times 10^3\,M_\odot$ and 5 pc, respectively. In the simulation, the multi-phase nature of ISM is realized by taking a wide temperature range of radiative cooling ($10 < T < 10^8$ K) and energy feedback from Type II supernovae (SNe) into account. Metal contamination of gas by Type II SNe is also taken into account (Steinmetz & Mueller 1994). Star formations take place from cold ($T < 100$ K) and dense ($n_{\rm H} > 100\,{\rm cm}^{-3}$) gas.

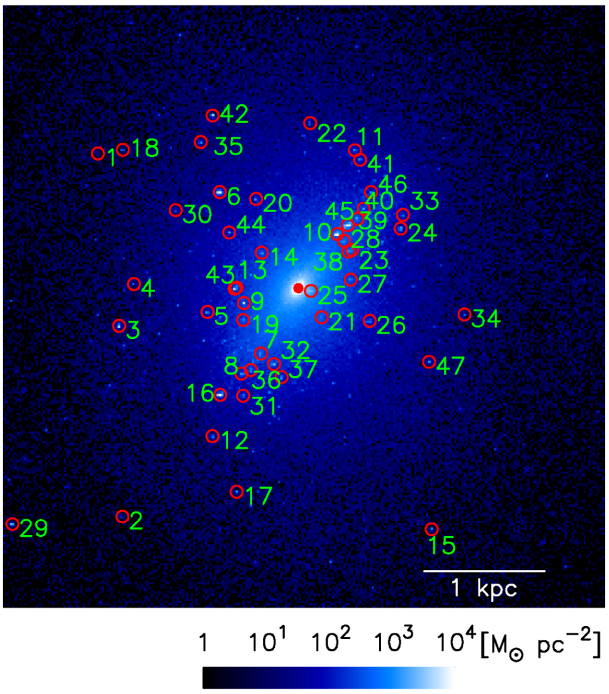

Fig. 1. Snapshot of both new stars and old stars in a merger remnant. The size of the panel is 5 kpc. The colors represent surface density of both new stars and old stars. A filled circle denotes the galactic center and open circles show detected YMCs. The numbers around the YMCs show the ID of the clusters. Although some faint dots can be observable in the other points, these objects cannot be identified as YMCs since they are gravitationally unbound or the cluster mass does not reach the detection limit mass. Two YMCs are not seen in this figure since these are much further from the galactic center. (Color online)

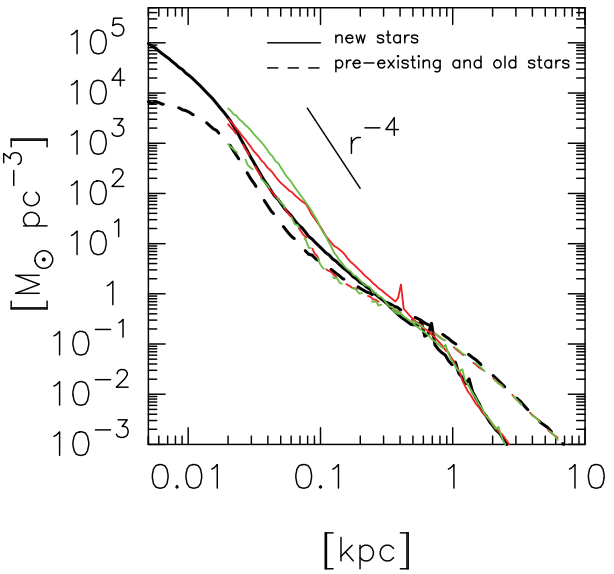

Fig. 2. Density profiles of young stars (solid lines) and pre-existing and old stars (dashed lines) in the merger remnants. Colored lines show simulation models of $H_{\mathrm{TT,\,5pc}}$ (black), H_{TT} (red), and L_{TT} (green). The red and green lines are not drawn within 20 pc since the gravitational softening length, namely spatial resolution, is 20 pc. (Color online)

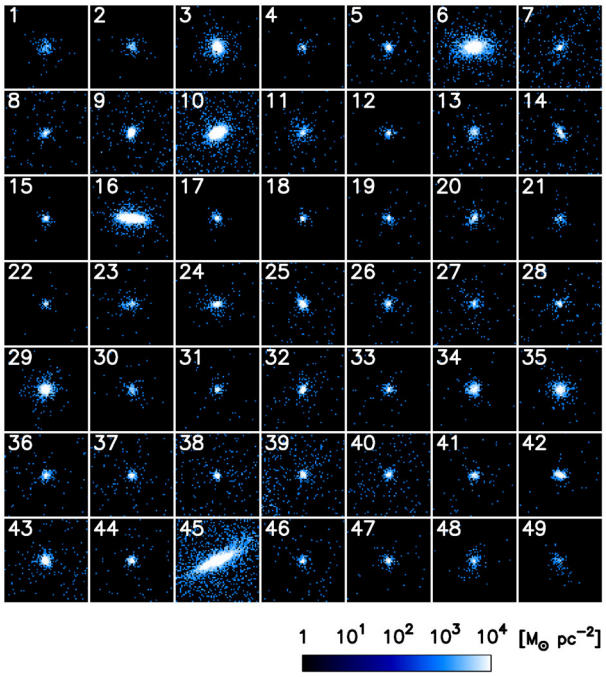

Fig. 3. Snapshots of detected YMCs. The size of each panel is 100 pc. The number displayed at the upper left in each panel shows the ID. (Color online)

The mass of a star particle spawned from an SPH is one third of the SPH mass.

In addition to the $H_{\mathrm{TT,\,5pc}}$ model, the lower resolution models H_{TT} and L_{TT} are also analyzed. These models have different mass and spatial resolutions from the $H_{\mathrm{TT,\,5pc}}$ model, but the same collision parameter. In the H_{TT} model, the gravitational softening length is 20 pc but the SPH mass is the same as for $H_{\mathrm{TT,\,5pc}}$. In the L_{TT} model, the SPH mass is $3 \times 10^4\,M_\odot$, and the gravitational softening length is 20 pc.

2.2 Identification of young massive clusters

We analyze simulation data at $t \sim 1350$ Myr. At that time, about 300 Myr passes after the galaxy merger is completed. We regard the lower limit of the detectable mass of the cluster as $2 \times 10^5\,M_\odot$ in $H_{\mathrm{TT,\,5pc}}$ and H_{TT} and as $8 \times 10^5\,M_\odot$ in L_{TT}, since clusters can be expressed by 100 new star particles.

In order to detect YMCs, we firstly compute the gravitational potential energy of old and new stars. After that calculation, we perform a gravitational bound check for old and new star particles around the particle with locally minimum potential. If particles are gravitationally bound and the total mass of the bound particles exceed the mass limit, we identify the system as a YMC.

Table 1. Property of YMCs in the $H_{\mathrm{TT,\,5pc}}$ case.

ID	M^* [$M_\odot$]	$r^\dagger$ [kpc]	$t_{25\%}{}^\ddagger$ [Myr]	$t_{50\%}{}^\S$ [Myr]	$t_{75\%}{}^\parallel$ [Myr]	$r_{\mathrm{p}}{}^\sharp$	$r_{\mathrm{a}}{}^{**}$	$\epsilon^{\dagger\dagger}$
1	3.14×10^5	2.01	−779	−778	−703	1.88	2.03	0.04
2	3.12×10^5	2.40	−845	−843	146	1.58	2.63	0.25
3	3.09×10^6	1.55	−369	298	832	0.65	1.69	0.45
4	2.23×10^5	1.38	742	743	744	1.37	1.82	0.14
5	6.43×10^5	0.81	1061	1062	1063	0.44	0.85	0.31
6	1.08×10^7	1.08	978	984	987	0.62	1.29	0.35
7	4.41×10^5	0.64	1238	1239	1240	0.55	0.68	0.11
8	4.02×10^5	0.88	1182	1183	1185	0.59	0.90	0.21
9	2.22×10^6	0.54	1030	1030	1032	0.53	0.88	0.25
10	2.46×10^7	0.58	1136	1180	1254	0.58	0.59	0.01
11	5.53×10^5	1.24	1181	1182	1183	1.05	1.32	0.11
12	3.68×10^5	1.58	1151	1153	1154	0.98	1.60	0.24
13	4.34×10^5	0.83	967	970	971	0.79	1.38	0.28
14	5.90×10^5	0.71	1068	1069	1070	0.60	0.74	0.10
15	4.17×10^5	2.39	1033	1034	1035	0.57	2.40	0.62
16	1.95×10^7	1.41	969	984	1011	0.25	1.70	0.75
17	3.93×10^5	2.51	952	953	954	1.02	2.54	0.43
18	3.28×10^5	2.29	705	706	707	0.95	2.72	0.48
19	3.26×10^5	1.21	1267	1268	1269	0.49	1.28	0.45
20	6.14×10^5	1.41	1098	1099	1101	0.83	1.46	0.27
21	2.22×10^5	1.36	1093	1102	1105	0.65	1.48	0.39
22	2.14×10^5	1.73	1058	1059	1060	1.21	1.86	0.21
23	3.55×10^5	1.24	1278	1279	1280	0.98	1.24	0.12
24	1.04×10^6	1.57	1100	1102	1104	0.96	1.58	0.25
25	1.15×10^6	0.88	1051	1053	1259	0.83	0.89	0.04
26	4.62×10^5	1.17	1166	1168	1169	0.84	1.23	0.19
27	3.54×10^5	1.05	1266	1269	1270	0.87	1.16	0.15
28	5.17×10^5	1.04	1318	1319	1321	0.89	1.12	0.11
29	2.41×10^6	3.17	−558	14	487	0.61	3.39	0.70
30	2.71×10^5	1.32	−839	−111	416	1.26	3.78	0.50
31	2.74×10^5	1.16	1154	1155	1157	0.82	1.23	0.20
32	8.76×10^5	0.91	1147	1149	1150	0.91	1.04	0.07
33	4.16×10^5	1.24	1115	1116	1117	0.73	1.24	0.26
34	1.09×10^6	1.50	−872	−870	−869	0.25	1.67	0.74
35	1.55×10^6	1.50	−871	−869	472	0.92	2.88	0.52
36	5.33×10^5	0.88	1182	1184	1185	0.62	0.91	0.19
37	5.81×10^5	0.78	1062	1063	1064	0.59	0.82	0.16
38	6.77×10^5	0.62	1197	1198	1199	0.31	0.71	0.40
39	6.44×10^5	0.80	1231	1232	1234	0.58	0.88	0.21

3 Results

3.1 Merger remnant

A snapshot of a merger remnant at $t \sim 1350$ Myr in the $H_{\mathrm{TT,\,5pc}}$ model is shown in figure 1. We detect 49 YMCs in the remnant.

Figure 2 shows the density profile of new stars and pre-existing and old stars in the merger remnant at $t \sim 1350$ Myr. The density profile of new stars is steep and declines as approximately $\rho \propto r^{-4}$ in an outer region larger than several tens of parsecs. The profile with r^{-4} is produced by the experience of strong gravitational disturbances (Makino et al. 1990). In the case of a galaxy merger, the intense disturbances are caused by the merging of galactic cores and the sinking of hypermassive star clusters through dynamical friction. Within 500 pc from the galactic center, new stars are dominant. The central density is much higher than that of both pre-existing and old stars by one order of magnitude. Such structures are compatible with extremely compact structures of newly formed stars observed in ultra-luminous infrared galaxies (ULIRGs) (Soifer et al. 2000; Mao et al. 2014).

The merger remnant has the total stellar mass of $1.2 \times 10^{10}\,M_\odot$ at that time. The V-band absolute magnitude M_{V}

Table 1. (Continued)

ID	M^* [$M_\odot$]	$r^\dagger$ [kpc]	$t_{25\%}{}^\ddagger$ [Myr]	$t_{50\%}{}^\S$ [Myr]	$t_{75\%}{}^\parallel$ [Myr]	$r_p{}^\sharp$	$r_a{}^{**}$	$\epsilon^{\dagger\dagger}$
40	5.82×10^5	0.90	1060	1061	1061	0.67	0.95	0.17
41	4.49×10^5	1.21	1169	1171	1172	1.13	1.29	0.06
42	1.62×10^6	1.62	950	950	951	0.32	3.47	0.83
43	1.80×10^6	0.53	1017	1019	1019	0.36	0.91	0.44
44	6.93×10^5	0.74	1022	1023	1023	0.26	1.59	0.72
45	4.51×10^7	0.69	1087	1145	1269	0.69	0.78	0.06
46	3.34×10^5	1.02	1176	1177	1178	0.94	1.39	0.19
47	4.91×10^5	1.25	875	876	876	0.62	1.42	0.39
48	4.07×10^5	11.30	817	819	820	11.04	18.67	0.26
49	2.08×10^5	9.31	762	765	766	9.07	17.63	0.32

*Mass of a YMC.
†Distance of a YMC from the center of the merger remnant.
‡Star formation time of a star located at 25% when stars within a YMC are sorted from young to old.
§Star formation time of a star located at 50% when stars within a YMC are sorted from young to old.
‖Star formation time of a star located at 75% when stars within a YMC are sorted from young to old.
♯Pericenter distance of a YMC.
**Apocenter distance of a YMC.
††Eccentricity of an orbit.

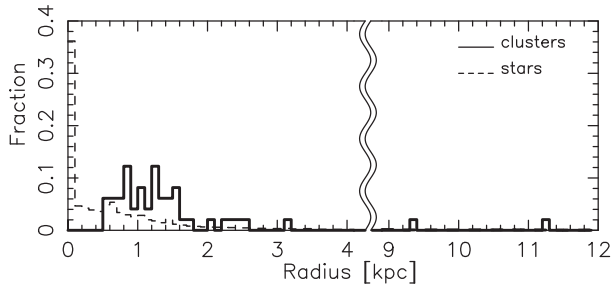

Fig. 4. Distribution of star clusters and new stars. The horizontal and vertical axes show the radius of the clusters from the center of the merger remnant and the number fraction of them, respectively. The graph has a bin width of 100 pc.

of the remnant is estimated by utilizing data of star particles and the population synthesis code PEGASE (Fioc & Rocca-Volmerange 1999). Then, $M_V = -19.8$ is obtained, so that the specific frequency, defined as $S_N = N_{cl} \times 10^{(M_V+15)}$ (Harris & van den Bergh 1981), is 0.61. Here, N_{cl} is the number of YMCs and $N_{cl} = 49$, and the effect of dust absorption is not taken into account. This value seems to be lower than that observed in dwarf ellipticals and is comparable to that of late-type galaxies (Miller et al. 1998). This is because only 300 Myr passes after galaxy–galaxy merging is completed and star particles are young, so the remnant is still bright. If star particles evolve further and the remnant becomes dark, the value is close to observed one. For example, when a further 1000 Myr passes, M_V and S_N become -18.9 and 1.4, respectively, assuming passive evolution.

3.2 Distribution of young massive clusters

All detected YMCs are shown in figure 3. The physical quantities of the clusters are listed in table 1. Figure 4 shows the fraction of YMCs and new stars in number as a function of radius from the galactic center. Most of the YMCs are located in a region a few kpc from the galactic center whereas new stars are extremely concentrated in the central region and nearly 40%of them are distributed within 100 pc. In H_{TT} and L_{TT} cases, the distribution of YMCs and new stars is similar to that of the $H_{TT,\,5pc}$ case, as shown in figure 2 and table 2. The difference in distribution between YMCs and stars in the galactic central region is consistent with observations (Sikkema et al. 2006) and can be explained as follows. YMCs form mainly from widespread gas filaments generated at the encounter of two galaxies or spatially extended turbulent gas generated by its inflow toward the galactic central region at the final coalescence phase of galactic cores. On the other hand, a large number of new stars are supplied by the sinking of hypermassive star clusters in addition to star formations from such compressed gas (Paper I). The formation epoch of YMCs in our simulations is different from that in Renaud, Bournaud, and Duc (2015), in which cluster formations mainly take place at the first encounter of galaxies. This would be due to the difference in collision parameters. In Renaud, Bournaud, and Duc (2015), an antennae-like collision parameter is adopted, which reproduces the compression of the gas and the formation of star clusters after the first encounter of galaxies.

Two of the clusters, IDs 48 and 49, appear at ∼10 kpc from the center of the merger remnant. These clusters are gravitationally bound by the remnant. Their formations

Table 2. Property of YMCs in H_{TT} and L_{TT} cases.*

ID	$M^{\dagger}$ [$M_{\odot}$]	$r^{\ddagger}$ [kpc]	$t_{25\%}{}^{\S}$ [Myr]	$t_{50\%}{}^{\|}$ [Myr]	$t_{75\%}{}^{\sharp}$ [Myr]	$r_{\rm p}{}^{**}$	$r_{\rm a}{}^{\dagger\dagger}$	$\epsilon^{\ddagger\ddagger}$
50	4.90×10^7	0.41	898	917	969	0.38	1.28	0.54
51	2.21×10^5	1.15	1173	1175	1177	1.09	1.22	0.06
52	2.02×10^6	1.06	1164	1166	1168	1.05	1.10	0.02
53	6.69×10^5	0.73	1195	1197	1198	0.69	0.73	0.03
54	1.63×10^6	2.97	897	901	903	0.08	3.03	0.95
55	9.90×10^5	1.37	917	918	919	0.77	1.43	0.30
56	4.45×10^6	1.16	889	897	900	0.75	1.46	0.32
57	2.69×10^6	0.84	1000	1001	1002	0.34	0.87	0.43
58	3.12×10^5	1.19	888	895	899	0.75	1.44	0.31
59	2.11×10^6	0.95	1025	1026	1027	0.94	1.08	0.07
60	9.40×10^6	1.21	1011	1015	1020	0.82	1.21	0.19
61	1.14×10^7	0.91	1200	1203	1314	0.75	0.91	0.10
62	3.88×10^6	2.24	883	885	913	0.17	3.44	0.91
63	9.72×10^5	0.90	1214	1215	1217	0.90	1.13	0.11

*YMCs from ID 50 to ID 59 and from ID 60 to ID 63 form in H_{TT} and L_{TT} cases, respectively.
†Mass of a YMC.
‡Distance of a YMC from the center of the merger remnant.
§Star formation time of a star located at 25% when stars within a YMC are sorted from young to old.
‖Star formation time of a star located at 50% when stars within a YMC are sorted from young to old.
♯Star formation time of a star located at 75% when stars within a YMC are sorted from young to old.
**Pericenter distance of a YMC.
††Apocenter distance of a YMC.
‡‡Eccentricity of an orbit.

take place in tidal tails away from the center, which is different from the formations of other clusters. These are classified as tidal dwarfs. In our simulations, there is no ejected YMC from the galaxy during galaxy–galaxy interaction as suggested by Elmegreen (2010). The difference of the formation site produces two components of YMC distribution. In H_{TT} and L_{TT} cases, the formation of a tidal dwarf does not occur.

In order to compare our data with observations, we show the surface number density of YMCs as a function of radius from the galactic center in figure 5. Here, the surface density is calculated by using projected snapshots which are observed from various viewpoints. The figure shows that the distribution of YMCs do not strongly depend on viewing angle. Whereas the stellar distribution traces the distribution of YMCs in the galactic outer region, the deficit of YMCs appears in the galactic inner region. This result is in agreement with observations of isolated elliptical galaxies (Sikkema et al. 2006; Salinas et al. 2015).

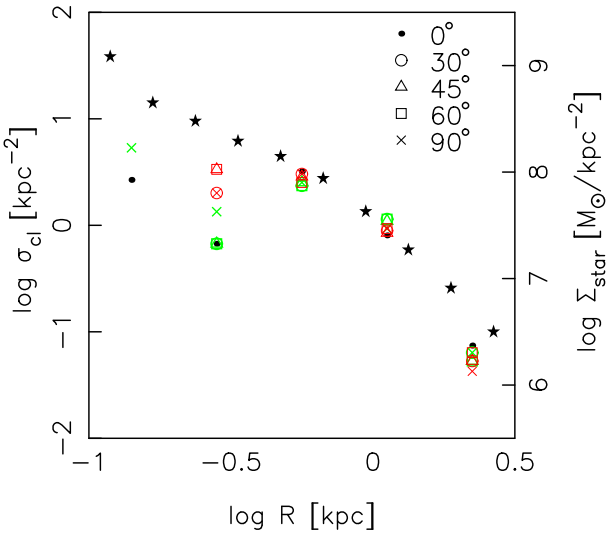

Fig. 5. Surface number density $\sigma_{\rm cl}$ of YMCs and surface new stellar mass density $\Sigma_{\rm star}$ as a function of radius from the galactic center. The bin width of $\sigma_{\rm cl}$ and $\Sigma_{\rm star}$ is 0.3 and 0.15, respectively. In order to obtain projected snapshots from various viewpoints, we rotate figure 1 with respect to its horizontal or vertical axis. The red and green plots show the horizontal and vertical cases, respectively. The viewpoints are indicated by different symbols ($\sigma_{\rm cl}$ = 0°, 30°, 45°, 60°, and 90°). The black star symbols denote $\Sigma_{\rm star}$. (Color online)

3.3 Mass function of young massive clusters

The cumulative mass function of YMCs is shown in figure 6. In the $H_{\rm TT,\,5pc}$ model, the masses of clusters range from 2.08 $\times 10^5\,M_{\odot}$ to 4.51 $\times 10^7\,M_{\odot}$. There are no hypermassive star clusters with $\sim 10^8\,M_{\odot}$ since they have already sunk to the galactic center through dynamical friction. This graph indicates that mass function becomes a power-law function with $dN/dM \propto M^{-2}$, which is in good agreement with observations (Whitmore et al. 1999) and previous numerical simulations (Saitoh et al. 2010).

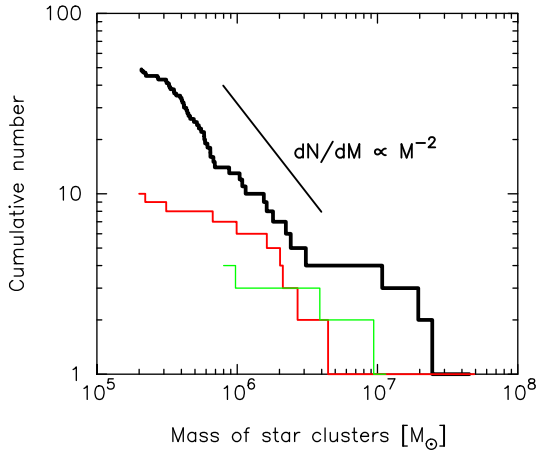

Fig. 6. Cumulative mass function. The vertical and horizontal axes are the cumulative number and mass of YMCs, respectively. Each line shows $H_{TT,\,5pc}$ (black), H_{TT} (red), and L_{TT} (green). (Color online)

A deviation from the line of $dN/dM \propto M^{-2}$, however, appears at $\sim 10^7\,M_\odot$; in other words, there is an excess of massive clusters. The stellar mass evolutions of massive YMCs IDs 10, 16, and 45 are shown in figure 7. The figure shows that their initial stellar masses are less than $\sim 10^7\,M_\odot$. After the formations of YMCs, these three YMCs continue to pass filamentary dense gas regions which exist within ~ 1 kpc from the galactic center. The YMCs obtain such dense gas continuously, and formations of new stars take place within the YMCs. As a result, stellar mass growth of the YMCs occurs and an excess of massive YMCs emerges. Since the cluster with ID 16 escapes from the dense gas region, mass growth is quenched at $t \sim 1030$ Myr. These objects seem to be more spatially extended (see figure 3) than observed young clusters which have a half-light radius of a few pc (Mengel et al. 2008). Such massive clusters would sink into the galactic center through dynamical friction within less than 1 Gyr, according to Chandrasekahr's formula:

$$t_{\rm dyn} = \frac{0.95\ {\rm Gyr}}{\ln \Lambda} \left(\frac{r}{0.5\ {\rm kpc}} \right)^2 \frac{\sigma}{200\ {\rm km\ s^{-1}}} \frac{2 \times 10^7\,M_\odot}{M} \quad (1)$$

(Binney & Tremaine 1987). Then, the excess disappears and spatially extended clusters would not be observed.

In the H_{TT} model, the mass function in the region less massive than $10^6\,M_\odot$ is deviated from $dN/dM \propto M^{-2}$. This is because the large gravitational softening length prevents the formations of clusters less than $10^6\,M_\odot$.

3.4 Age of young massive clusters

In table 1, $t_{XX\%}$ indicates the time when XX% of stars in each cluster are formed. According to $t_{25\%}$, $t_{50\%}$, and $t_{75\%}$, the clusters can be classified into the following three types: (1) clusters consisting of only new stars with single age, (2) clusters consisting of only new stars with bimodal distribution in age, (3) massive clusters consisting of only new stars with varying age, and (4) clusters constituting of both new and old stars.

38 YMCs consist of only new stars with single age. All of these clusters form after galaxy–galaxy encounters, and their formations are induced by the galaxy merger. The typical population of stellar age within these clusters is shown in the left-hand panel of figure 8 which shows the number fraction of stars within a cluster as a function of star formation time. Stars within these clusters have similar formation epochs and the width of age distribution is 10 Myr, which is the timescale of feedback to eject gas.

One YMC, ID 25, has bimodal distribution in age as shown in the middle panel of figure 8. The interval of age between the two events is 200 Myr. The process of producing such a population is as follows. The cluster forms at $t = 1050$ Myr. After the formation, the cluster wanders few gas regions. When the cluster passes the dense gas region temporarily after $t \sim 1250$ Myr, it captures gas, as shown in the left-hand and middle panels of figure 9. After that, the density of gas within the cluster becomes high and gas cools because of the radiative cooling. As a result, the next-generation stars form, as shown in the right-hand panel of figure 9. This scenario has been suggested by Pflamm-Altenburg and Kroupa (2009).

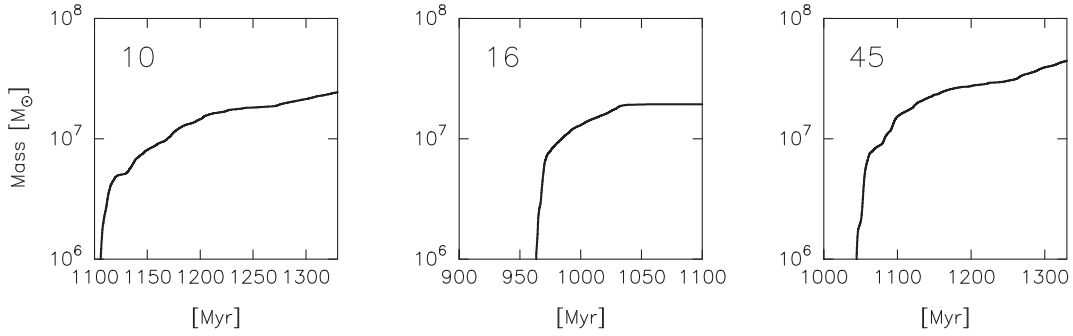

Fig. 7. Time evolutions of stellar mass of massive YMCs for IDs 10, 16, and 45.

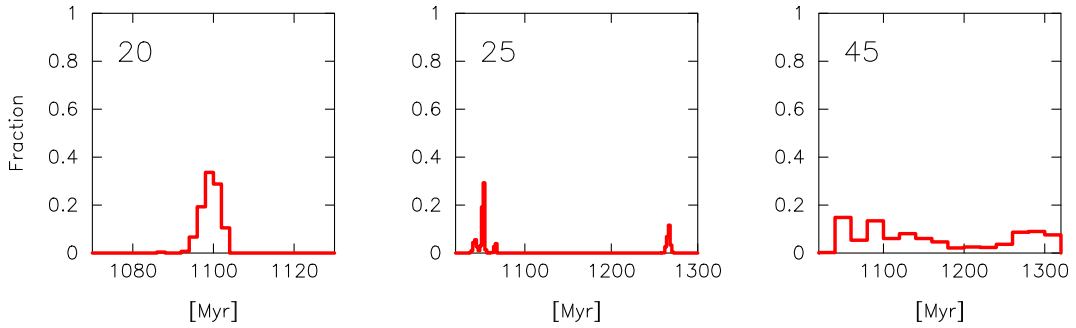

Fig. 8. Distribution of star formation time in each YMC formed after the galaxy encounter. The horizontal and vertical axes are the star formation time and the number fraction of stars to the total stellar number, respectively. The number in the upper left-hand corner denotes the cluster ID. (Color online)

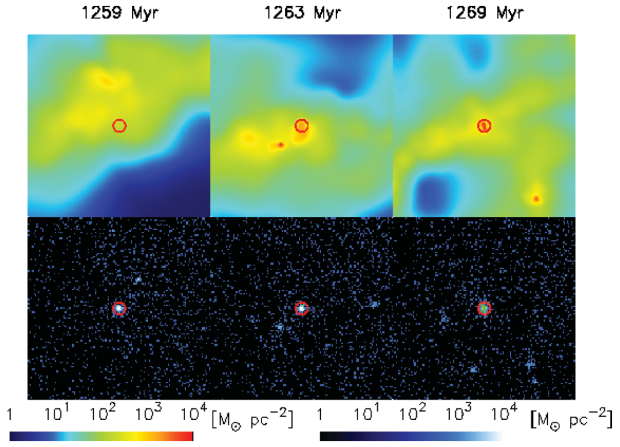

Fig. 9. Snapshots of the cluster ID 25 from $t = 1259$ Myr to $t = 1269$ Myr. Top and bottom panels show the surface density of the gas and the new star, respectively. The red circle represents the position of the cluster. In the bottom panels, green dots represent formed next-generation stars. At $t = 1259$, a dense gas region appears above the cluster. After that, the cluster passes through this region. Then, the cluster captures gas at $t = 1263$ Myr and star formation takes place within the cluster. (Color online)

Three YMCs, IDs 10, 16, and 45, exceed $10^7\,M_\odot$. These clusters consist of stars with various ages. The typical distribution of the stellar formation time is shown in the right-hand panel of figure 8. The distribution is continuous rather than discrete, unlike ID 25. This is because these YMCs continue to pass dense gas regions and obtain gas continuously. The continuous gas accretion results in star formations within the clusters at various times.

The other seven YMCs consist of old and new stars, although the clusters ID 1 and ID 34 have few new stars. All of these seven clusters form in an initial unstable gas disk at $t \sim -800$ Myr during a simulation of an isolated gas disk. Figure 10 shows the distribution of the formation time of stars within these clusters. Although these clusters form in an initial isolated unstable gas disk at $t \sim -800$ Myr, they include stars with various formation times. This is because clusters capture gas when they pass through dense gas regions and star formations occur within them, similarly to the cluster ID 25. These clusters are likely to contain stars formed at the encounter phase, namely around 400 Myr or 800 Myr. The reason is that the encounter produces turbulent and dense gas and increases the probability that a cluster passes through the dense gas region.

In $H_{\rm TT}$ and $L_{\rm TT}$ cases, $t_{25\%}$, $t_{50\%}$, and $t_{75\%}$ are shown in table 2. All YMCs form after the second encounter of galaxies. Whereas most YMCs have a single stellar population, IDs 50, 61, and 62 have multiple stellar populations. ID 50 and ID 62 consist of stars with various ages, similarly to IDs 10, 16, and 45, and ID 61 has a bimodal stellar population in age, similarly to ID 25. The multiple population is formed by capturing dense gas and forming the second-generation stars in a similar way to the $H_{\rm TT,5pc}$ case.

Recent observations have revealed that Galactic globular clusters generally have multiple stellar populations (Bastian & Lardo 2017). Such globular clusters can be divided into two types in accordance with abundance patterns. The first and second types contain Fe and light element (e.g., He, C, N, O, Na, and Al) variations. Since we do not have abundance information for stars in our simulation, we conjecture types of YMCs with bimodal distribution in age. These YMCs should belong to the first type for the following reasons. These YMCs, except ID 25, contain stellar populations formed before and after the galaxy–galaxy merger. These stellar populations clearly have different Fe abundances. YMC ID 25 has stellar populations formed at $t \sim 1050$ Myr and $t \sim 1250$ Myr. The metallicity, Z, of the first- and second-generation stars in YMC ID 25 is shown in figure 11. The figure shows that the metallicity of the second-generation stars increases by $\sim$0.01 compared to that of first-generation stars. Although the enrichment

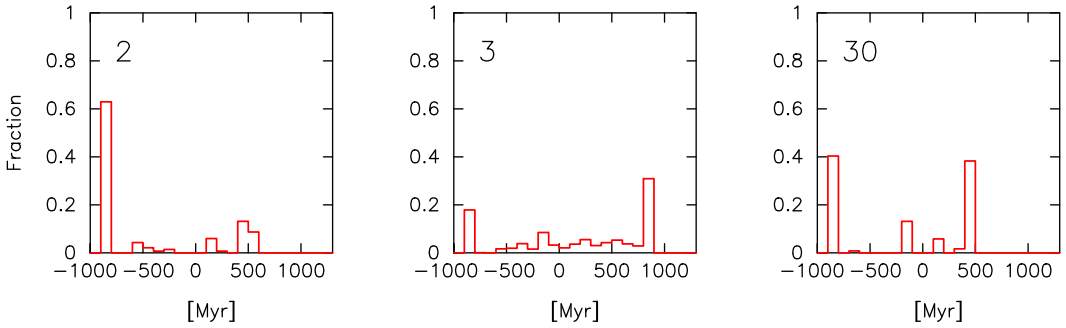

Fig. 10. Same as figure 8 but clusters formed before the galaxy encounter. (Color online)

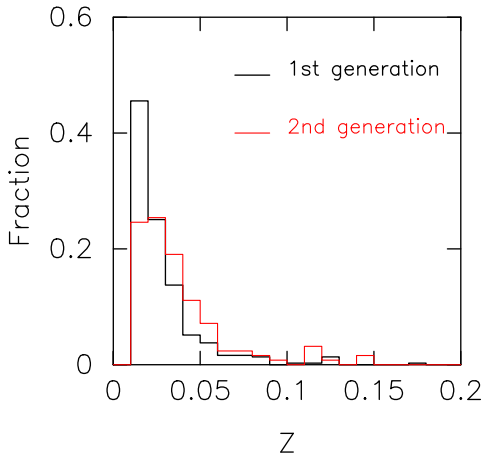

Fig. 11. Number fraction of stars as a function of metallicity Z in the cluster with ID 25. The black and red lines show the first- and the second-generation stars, respectively. The bin width is 0.01. (Color online)

seems to be mild, it becomes more remarkable in high-z galaxies with low metallicity. The difference of metallicity between the first- and second-generation stars indicates that the second-generation stars form from gas contaminated by Type II SNe. Thus, these clusters correspond to ω Cen with different Fe abundances. On the other hand, the second type is expected to be formed from asymptotic giant branch (AGB) ejecta of the first-generation stars (Renzini 2008; Bekki et al. 2017; Bekki 2018).

3.5 Motion of young massive clusters

In order to investigate orbits of YMCs in the merger remnant, we simulate the motion of YMCs by the second-order leapfrog integration scheme. The gravitational potential of the remnant is produced by using the distribution of SPH, star, and dark matter particles at $t \sim 1350$ Myr. Here, we assume that the gravitational potential is steady and spherically symmetric. These assumptions are reasonable to calculate orbits approximately since the asymmetry of the remnant is not strong and the remnant is quasi-stable. Note that evaporation of YMCs and dynamical friction are not taken account.

The pericenter distance $r_{\rm p}$, apocenter distance $r_{\rm a}$, and eccentricity defined by $\epsilon = (r_{\rm a} - r_{\rm p})/(r_{\rm a} + r_{\rm p})$ are summarized in table 1 for the high-resolution case and in table 2 for the low-resolution cases. In both cases, orbits of YMCs in the galactic inner region are various, but the number fraction of circular orbits is large. This is because YMCs formed in a major merger do not lose the orbital angular momentum sufficiently. This trend seems to be different from observations of the Milky Way (Gaia Collaboration 2018) or cosmological simulations of a disk galaxy (Saitoh et al. 2006) which is different morphology from a galaxy–galaxy merger remnant and does not experience a recent major merger. Such observations and simulations show that a large fraction of YMCs have radial orbits. This might indicate that the formation process of clusters is different between a merging galaxy and a disk galaxy. While YMCs form from filamentary gas or turbulent gas generated by a galaxy–galaxy merger, YMCs form by in situ formation, minor mergers, and satellite accretion (Renaud et al. 2017).

Eccentricities of orbits of the galactic outer YMCs ID 48 and ID 49 are not high. This is because they form in rotating tidal tails and hence have originally sufficient orbital angular momentum. These clusters migrate from $\sim$10 kpc to $\sim$20 kpc. Since their pericenter and apocenter distances are $\sim$10 kpc and $\sim$20 kpc, respectively, these objects are observed as isolated globular clusters. Isolated globular clusters are observed in some galaxies, for examples M 31 (Mackey et al. 2010) and M 81 (Jang et al. 2012), although it is difficult to compare simply with spiral galaxies.

4 Summary

We investigate properties of YMCs in a merger remnant by analyzing simulation data in Paper I. Our findings are as follows.

- YMCs are formed in filamentary and turbulent gas and tidal tails generated by a galaxy merger. The former and the latter are distributed at a few kpc and at $\sim$10 kpc from the center of the merger remnant, respectively. The YMCs are much less concentrated than galaxy stars.
- The mass function of YMCs becomes $dN/dM \propto M^{-2}$, but the excess appears around $10^7\,M_\odot$ after merging of galactic cores is completed. The excess would disappear after less than 1 Gyr due to dynamical friction.
- Most YMCs formed during a galaxy merger consist of a single stellar population in age. On the other hand, the rest have multiple distributions in age. The multiple population is formed by capturing dense gas and forming new stars within a YMC when the YMC passes a dense gas region.
- Orbits of YMCs in the inner galactic region are various, but a large fraction of candidates would more likely have circular orbits. Eccentricities of YMCs in the inner galactic region are not high.

Acknowledgment

We thank Dr. Florent Renaud for giving us useful comments. Numerical computations were carried out on Cray XT4 at Center for Computational Astrophysics (CfCA), National Astronomical Observatory of Japan, and numerical analyses were carried out on computers at CfCA, National Astronomical Observatory of Japan. This research has been supported in part by the MEXT programme for the Development and Improvement for the Next Generation Ultra High-Speed Computer System under its Subsidies for Operating the Specific Advanced Large Research Facilities, and by Grants-in-Aid for Scientific Research (16K17656, 17H06360) from the Japan Society for the Promotion of Science.

References

Barnes, J. E., & Hernquist, L. 1996, ApJ, 471, 115
Bassino, L. P., & Caso, J. P. 2017, MNRAS, 466, 4259
Bastian, N., & Lardo, C. 2018, ARA&A, 56, 83
Bekki, K. 2018, arXiv:1807.02309
Bekki, K., Forbes, D. A., Beasley, M. A., & Couch, W. J. 2002, MNRAS, 335, 1176
Bekki, K., Jeřábková, T., & Kroupa, P. 2017, MNRAS, 471, 2242
Binney, J., & Tremaine, S. 1987, Galactic Dynamics (Princeton: Princeton University Press)
Bournaud, F., Duc, P.-A., & Emsellem, E. 2008, MNRAS, 389, L8
Choudhury, S., Subramaniam, A., & Cole, A. A. 2016, MNRAS, 455, 1855
Cox, T. J., Dutta, S. N., Di Matteo, T., Hernquist, L., Hopkins, P. F., Robertson, B., & Springel, V. 2006, ApJ, 650, 791
Di Matteo, P. Combes F., Melchior, A.-L., & Semelin, B. 2007, A&A, 468, 61
Elmegreen, B. G. 2010, ApJ, 712, L184
Fioc, M., & Rocca-Volmerange, B. 1999, arXiv:astro-ph/9912179
Gaia Collaboration, 2018, A&A, 616, A12
Harris, W. E., & van den Bergh, S. 1981, AJ, 86, 1627
Hopkins, P. F., Cox, T. J., Hernquist, L., Narayanan, D., Hayward, C. C., & Murray, N. 2013a, MNRAS, 430, 1901
Hopkins, P. F., Kereš, D., Murray, N., Hernquist, L., Narayanan, D., & Hayward, C. C. 2013b, MNRAS, 433, 78
Jang, I. S., Lim, S., Park, H. S., & Lee, M. G. 2012, ApJ, 751, L19
Kaneko, H., Kuno, N., & Saitoh, T. R. 2018, ApJ, 860, L14
Kazantzidis, S., et al. 2005, ApJ, 623, L67
Kim, J.-h., et al. 2018, MNRAS, 474, 4232
Kim, J.-h., Wise, J. H., & Abel, T. 2009, ApJ, 694, L123
Ko, Y., Lee, M. G., Park, H. S., Sohn, J., Lim, S., & Hwang, N. 2018, ApJ, 859, 108
Kruijssen, J. M. D., Pelupessy, F. I., Lamers, H. J. G. L. M., Portegies Zwart, S. F., Bastian, N., & Icke, V. 2012, MNRAS, 421, 1927
Mackey, A. D., et al. 2010, MNRAS, 401, 533
Makino, J., Akiyama, K., & Sugimoto, D. 1990, PASJ, 42, 205
Mao, M. Y., Norris, R. P., Emonts, B., Sharp, R., Feain, I., Chow, K., Lenc, E., & Stevens, J. 2014, MNRAS, 440, L31
Matsui, H., et al. 2012, ApJ, 746, 26 (Paper I)
Mengel, S., Lehnert, M. D., Thatte, N. A., Vacca, W. D., Whitmore, B., & Chandar, R. 2008, A&A, 489, 1091
Mihos, J. C., & Hernquist, L. 1996, ApJ, 464, 641
Miller, B. W., Lotz, J. M., Ferguson, H. C., Stiavelli, M., & Whitmore, B. C. 1998, ApJ, 508, L133
Pflamm-Altenburg, J., & Kroupa, P. 2009, MNRAS, 397, 488
Renaud, F., Agertz, O., & Gieles, M. 2017, MNRAS, 465, 3622
Renaud, F., Bournaud, F., & Duc, P.-A. 2015, MNRAS, 446, 2038
Renzini, A. 2008, MNRAS, 391, 354
Saitoh, T. R., Daisaka, H., Kokubo, E., Makino, J., Okamoto, T., Tomisaka, K., Wada, K., & Yoshida, N. 2008, PASJ, 60, 667
Saitoh, T. R., Daisaka, H., Kokubo, E., Makino, J., Okamoto, T., Tomisaka, K., Wada, K., & Yoshida, N. 2009, PASJ, 61, 481
Saitoh, T. R., Daisaka, H., Kokubo, E., Makino, J., Oakmoto, T., Tomisaka, K., Wada, K., & Yoshida, N. 2010, ASP Conf. Ser. 423, 185
Saitoh, T. R., Koda, J., Okamoto, T., Wada, K., & Habe, A. 2006, ApJ, 640, 22
Salinas, R., Alabi, A., Richtler, T., & Lane, R. R. 2015, A&A, 577, A59
Sikkema, G., Peletier, R. F., Carter, D., Valentijn, E. A., & Balcells, M. 2006, A&A, 458, 53
Soifer, B. T., et al. 2000, AJ, 119, 509
Steinmetz, M., & Mueller, E. 1994, A&A, 281, L97
Teyssier, R., Chapon, D., & Bournaud, F. 2010, ApJ, 720, L149
Whitmore, B. C., & Schweizer, F. 1995, AJ, 109, 960
Whitmore, B. C., Zhang, Q., Leitherer, C., Fall, S. M., Schweizer, F., & Miller, B. W. 1999, AJ, 118, 1551